Nanoscale

Cite this: *Nanoscale*, 2011, **3**, 3238

www.rsc.org/nanoscale

PAPER

Heterostructured CIGS–Au nanoparticles: from Au–CIGS side-by-side structure to Au-core/CIGS-shell configuration†

Yeming Xu and Quan Li*

Received 12th March 2011, Accepted 16th May 2011
DOI: 10.1039/c1nr10268k

Heterostructured Au–Copper Indium Gallium Selenide (CIGS) nanoparticles (nps) with Au–CIGS side-by-side and Au-core/CIGS-shell configurations have been synthesized in a controllable manner using seed mediated growth. Detailed microstructure analysis reveals that (112) planes in the tetragonal chalcopyrite CIGS serve as the predominant termination surfaces during single phase CIGS nanoparticle growth. Preferential nucleation of Au on such planes determines the Au–CIGS side-by-side configuration when the pre-synthesized CIGS nps are used as the seeds for further Au growth. Reversing the growth sequence by employing Au nano-seeds results in Au-core/CIGS-shell configuration, as determined by the non-preferential nucleation of CIGS on the spherical Au nanoparticle surface. The different morphological configurations of the heterostructures are found to modify the surface plasmon resonance of Au in the corresponding samples.

Introduction

Metal–semiconductor heterostructured nanomaterials can integrate different functionalities of each individual component, and coupling between the metal and the semiconductor may further enhance specific properties or even bring entirely different ones that are sensitively dependent on both the type of materials and the specific configuration of the heterostructures. For example, enhanced charge carrier separation has been achieved in Au/CdSe bi-crystalline nanoparticles (nps) as the Au serves as an electron attracting center, and electrons can be further let out *via* medium surrounding the Au.[1] As a comparison, the Au-core/TiO_2-shell configuration fails to have such a property, as the accumulated charges in the Au core do not have a pathway to be consumed.[2] Another example is possible light absorption enhancement in semiconductors realized *via* a metal–semiconductor heterostructured system—the noble metal surface plasmon resonance (SPR) is known to generate an enhanced local electromagnetic field for the semiconductor absorption enhancement.[3] In order to achieve the maximum enhancement effect, a match between the semiconductor absorption energy and noble metal SPR is required, with the later energy value being affected by the heterostructured configuration.[4] Therefore, synthesis of metal/semiconductor nano-heterostructures in a controllable manner is of great research interest.[5]

Ternary/quaternary I–III–VI_2 chalcopyrite semiconductors, particularly copper indium gallium selenides ($CuIn_{(1-x)}Ga_xSe_2$; CIGS), have direct band gap in the visible absorption range, and thus become one of the most promising candidates for solar energy conversion applications.[6] Indeed, the conversion efficiency of thin film CIGS solar cells has already reached a record high of 20.3%.[7] In recent years, interest has also been generated in CIGS nanoparticle (np) based photovoltaic devices due to the development of low cost ink printing techniques, and a highest energy conversion efficiency of ~16.4% has been announced.[8] Coupling of CIGS and metallic nps may lead to improved optical and electronic properties, and such coupled heterostructure is expected to be a promising candidate for various photovoltaic and photocatalytic applications.[3,9,10] In fact, the consumption of In in CIGS solar cells is considered as unfavourable, as In is a rare element on earth. By coupling Au with CIGS and forming appropriate nano-heterostructures, one can enhance the absorption of the semiconductor, so as to reduce the usage of the CIGS, and consequently the rare element In without sacrificing the energy conversion efficiency of the device. Unfortunately, unlike many binary semiconductor/metal systems,[2,3,9–13] synthesis of metal–CIGS heterostructures with controllable morphologies is not available to date.

In this study, we demonstrate the morphology differentiation in Au–CIGS nanostructures by designing the growth route. Taking CIGS nps as the seeds, Au–CIGS side-by-side nps are obtained, while reversing the growth sequence (using Au nps for seeding) leads to the formation of Au-core/CIGS-shell heterostructures. The formation mechanisms of these heterostructured Au–CIGS nps are discussed in detail based on the nanoparticle microstructure analysis. The different configuration of the heterostructured Au–CIGS nps is found to affect the SPR of Au, as

Department of Physics, The Chinese University of Hong Kong, Shatin, New Territory, Hong Kong. E-mail: liquan@phy.cuhk.edu.hk

† Electronic supplementary information (ESI) available: The schematic of the (112) planes of CIS tetragonal chalcopyrite structure and various Au–CIGS side-by-side heterostructures (including one-to-one and multiple-to-one morphologies, which were synthesized at modified conditions). See DOI: 10.1039/c1nr10268k

suggested by the optical absorption measurements taken from the corresponding samples.

Experimental section

CIGS nanocrystals synthesis

The CIGS nanocrystals are synthesized using the literature reported method with modified parameters.[14,15] Briefly, 0.1 g CuCl, 0.11 g $InCl_3$, 0.21 g $Ga(NO_3)_3 \cdot 9H_2O$ and 15 mL oleylamine are introduced into a 50 mL three-necked round-bottom flask at room temperature. The flask is connected to a Schlenk line and placed on a heating mantle. Purging of oxygen and water from the solution is realized by rough vacuuming the system, followed by N_2 bubbling at 120 °C several times. The temperature is then increased to 240 °C and 5 mL oleylamine with 0.158 g Se are added into the flask. The reaction is kept at 240 °C with vigorous stirring under N_2 bubbling for 20 minutes. At last, 40 mL ethanol is added to the solution when the reaction is terminated and the CIGS nanocrystals precipitate out from the solution.

The nanocrystals are then re-dispersed in 30 mL chloroform and centrifuged at 10000 rpm for 5 min. The precipitate is discarded and the supernatant (containing nanocrystals of smaller size and more uniform size distribution) is used for further experiments.

Growth of Au–CIGS side-by-side nanocrystals

The chloroform supernatant obtained from the above procedures is introduced into a 50 mL three-necked flask and heated to ~62 °C (bp of chloroform) under vigorous stirring. Thereafter, 6 mL solution mixed with 50 mg $HAuCl_4 \cdot xH_2O$, 3 mL chloroform and 3 mL oleylamine is added into the system. The reaction proceeds for 5 h before being cooled down to room temperature. The nanocrystals are washed three times using excessive ethanol to remove extra surfactant.

Growth of Au-core/CIGS-shell structures

In a typical procedure, 0.11 g $In(acac)_3$, 0.21 g $Ga(acac)_3$, 0.13 g $Cu(acac)_2$, 15 mL dichlorobenzene (DCB) and 3 mL oleylamine are mixed at room temperature in a three-necked flask. The flask is evacuated to rough vacuum condition at 60 °C for 30 min, followed by N_2 bubbling for 10 min. The mixture is then heated to 120 °C under N_2 atmosphere. Mixtures of 3 mL DCB and 1 mL oleylamine containing 50 mg of $HAuCl_4 \cdot xH_2O$ are added to the flask. The reaction is kept at 120 °C for 10 min for Au seeds formation. After that 0.12 g selenourea dissolved in the solution of 3 mL DCB and 1 mL oleylamine are added to the flask for $CuIn_{(1-x)}Ga_xSe_2$ shell growth. The temperature is increased to 180 °C and kept for 1 h under vigorous stirring. Subsequently, the system is cooled down to room temperature, when ~10 mL methanol is added to quench the reaction and the nanocrystals precipitate. The nanocrystals are washed three times using ethanol.

The chemical composition and the structure of the CIGS nanocrystals and Au/CIGS heterostructures are investigated using X-ray diffraction (XRD, Rigakau RU-300 with $CuK\alpha_1$ radiation), scanning electron microscopy (FEG-SEM, Quanta 400F) and transmission electron microscopy (TEM, Tecnai F20) with an energy dispersive X-ray (EDX) spectrometer. For TEM-related analysis, samples are dispersed on carbon coated copper and gold grids. In measuring the composition of Cu, In, Ga and Se using TEM-EDX, the Au grid is used to avoid the Cu background signal from the Cu grid. On the other hand, the copper grid is used in investigating the Au existence in corresponding heterostructures. Ethanol suspensions of the nanoparticles are prepared for UV-Vis absorption analysis (Hitachi U-3501 UV-Vis-NIR spectrometer).

Results

We start with the description of pure CIGS nanoparticles. Fig. 1 (a) shows a low magnification TEM image of the CIGS nanoparticles with an average diameter of ~22 nm. A standard deviation of 11% can be estimated from the particle size distribution histogram in Fig. 1(b), based on several hundreds of nanoparticles counted from a number of low magnification TEM images. EDX taken from such CIGS nanoparticles (Fig. 1(c)) suggests an elemental ratio of Cu/In/Ga/Se close to 1/0.8/0.2/2 (a 5% error is associated with the EDX measurement). In fact, the Ga content in the sample can be varied by controlling the Ga source during synthesis[15] and we have obtained a series of CIGS nanoparticles with different Ga/In ratios. For simplicity, we take the above mentioned composition as an example.

The XRD pattern (Fig. 1(d)) of the as-synthesized $CuIn_{(1-x)}Ga_xSe_2$ nanocrystals can be indexed to the tetragonal chalcopyrite structure (JCPDS No. 40-1487 for pure CIS, 35-1100 for CGS, peak shifting occurs as the Ga concentration increases from CIS to CGS), and no peak corresponding to other phases is identified. The size of the crystals in the sample can be estimated as ~20 nm using the Scherrer equation,[16] agreeing well with the TEM observation. High-resolution electron microscopy has been

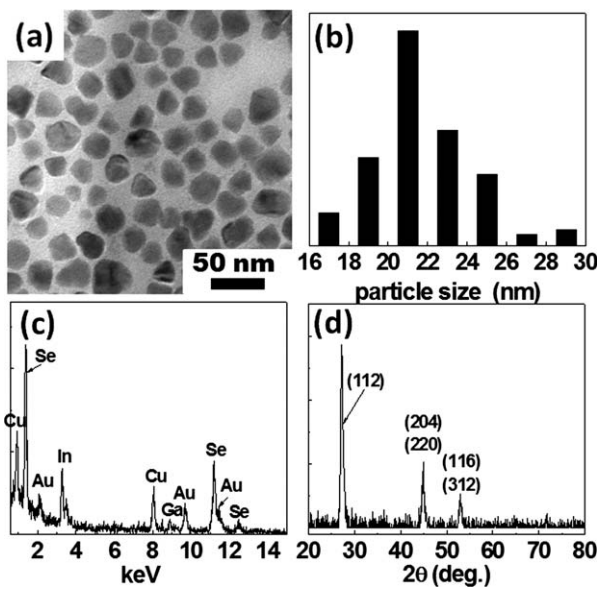

Fig. 1 (a) Low magnification TEM image of mono-dispersed CIGS particles; (b) size distribution histogram of CIGS nps; (c) EDX taken from a single particle (Au TEM grid is used); and (d) XRD taken from the CIGS nps powder.

carried out on several tens of individual nanoparticles, in order to investigate their crystallinity and termination surfaces. All of the individual nanoparticles are identified to be single crystalline with the tetragonal chalcopyrite structure.

Several typical high-resolution images of the individual particles are selected and shown in Fig. 2. It has been found that the crystalline (112) planes serve as predominant termination surfaces for these nanoparticles—most of them employ at least one, or in many cases, more than one (112) plane as their surfaces (Fig. 2(a)–(c)). Although some particles appear to be spherical without any specific crystalline plane as the termination surface (Fig. 2(d)), they are very rare.

Using the as-synthesized CIGS nanoparticles as the seeds for further Au growth, Au–CIGS side-by-side heterostructured nanoparticles can be obtained. Fig. 3(a) shows a typical low magnification TEM image taken from such a sample. The light/dark contrast can be clearly observed in individual particles due to the significant mass difference between Au and CIGS. The statistical yield of the heterostructured nanoparticles is estimated as 72% based on hundreds of nanoparticles counted from TEM. It is interesting to note that only one Au nanoparticle is adhered to one CIGS nanoparticle (Fig. 3(b)) in most cases. In an enlarged TEM image showing a single Au–CIGS nanoparticle (Fig. 3(b)), one would notice that the contact angle between Au and CIGS is always greater than 90 degrees, suggesting the non-wetting nature of Au with the CIGS surface(s). The EDX spectrum taken from such nanoparticles (Fig. 3(c)) shows the co-existence of Au, Cu, In, Ga, and Se signals. The presence of crystalline Au and the intactness of the crystalline chalcopyrite CIGS are suggested by the XRD pattern taken from the sample (Fig. 3(d)), in which no peak from another phase is found.

In order to investigate the interface between the Au and the CIGS in the side-by-side heterostructure, high-resolution TEM images are taken from several tens of nanoparticles, specifically

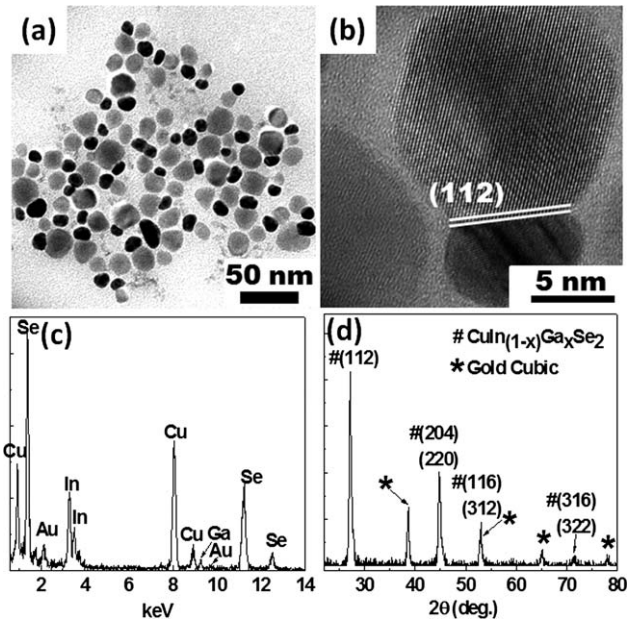

Fig. 3 (a) Low magnification TEM image of Au–CIGS side-by-side nanoparticles; (b) high resolution TEM image of one Au/CIGS particle; (c) EDX taken from a single heterostructured nanoparticle (Cu TEM grid is used for the observation of Au). The composition of CIGS can be estimated from sample dispersed on a Au TEM grid (Fig. S1(a)†); and (d) XRD taken from the powder sample of Au–CIGS side-by-side nps.

at the interface between Au and CIGS. Fig. 4 gives four typical examples at the interface. For all of the nanoparticles examined, Au is found to grow mostly on the (112) surface of the CIGS nanoparticles with a fairly sharp interface between the two. Nevertheless, no specific Au crystalline plane is found to interface with the CIGS, let alone any fixed epitaxial relationship between the two being observed.

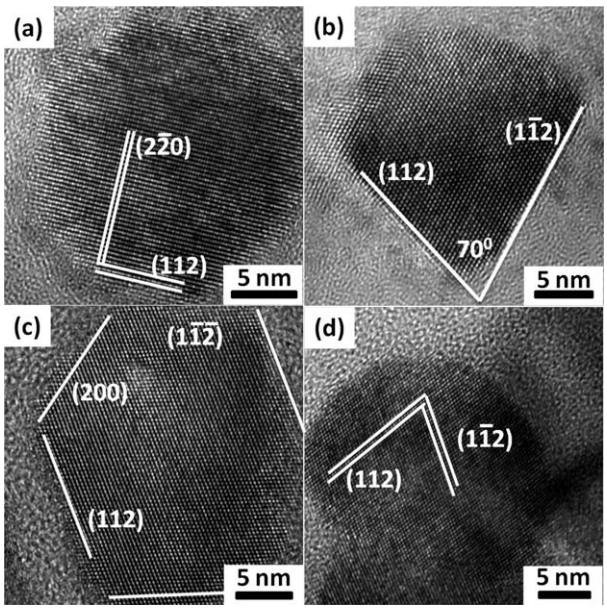

Fig. 2 (a)–(c) High resolution TEM images of individual CIGS nanoparticles with one or more (112) termination surfaces; and (d) a spherical CIGS np without any specific termination surface.

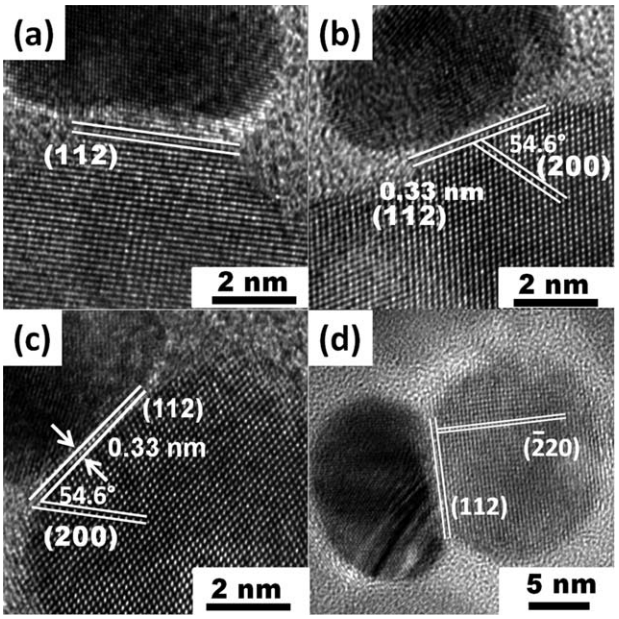

Fig. 4 (a)–(d) High-resolution TEM images showing the interfaces of four typical Au–CIGS side-by-side heterostructured nanoparticles.

By reversing the growth sequence, *i.e.*, using the pre-synthesized Au nanoparticle as the seeds for further CIGS growth, Au-core/CIGS-shell structure can be obtained. The morphology of the core/shell nanocrystals is revealed by the low magnification TEM image shown in Fig. 5(a). The dark and light contrast can be observed in the nanoparticle core and shell regions, respectively, again due to the mass difference between the two materials. The core/shell heterostructured particles have a 90% yield, which is obtained by counting hundreds of nanoparticles in TEM. The diameter of the Au core is ~10 to 15 nm, and the shell thickness in the range of 10–20 nm. The longer growth duration of CIGS would result in thicker shells. The EDX spectrum (Fig. 5 (b)) taken from such a sample is very similar to that of the Au–CIGS side-by-side structure, when all of the Au, Cu, In, Ga and Se signals are found to co-exist. The XRD pattern (Fig. 5(c)) taken from the core–shell nanoparticles confirms the co-existence of the cubic gold and the chalcopyrite CIGS. A magnified TEM image of a core–shell nanoparticle is shown in Fig. 5(d), in which the polycrystalline nature of the CIGS shell is clearly disclosed (Fig. S2†).

The absorptions of the samples are investigated by UV-Vis spectroscopy. Fig. 6 compares the room temperature UV-Vis absorbance spectra of (a) as-synthesized CIGS nps, (b) Au nps, (c) Au–CIGS side-by side nps, and (d) Au-core/CIGS-shell nps. In the case of pure CIGS nanoparticles, its band gap is estimated as ~1.17 eV by extrapolating the linear portion of the α^2 plot to the energy axis (inset of Fig. 6(a)).[17] This value agrees well with the calculated bulk $Cu_1In_{0.8}Ga_{0.2}Se_2$ (ratio obtained from the EDX results) band gap energy (~1.11 eV).[18] The absorption spectrum taken from pure gold nanoparticles (spherical gold particles with 10–15 nm size in diameter dispersed in hexane) shows an intense peak at ~520 nm due to the Au nanoparticle surface plasmon resonance (Fig. 6(b)). The formation of Au–CIGS side-by-side heterostructure results in a small red shift of the SPR from 520 nm to ~540 nm (Fig. 6(c)). As a comparison, a significant redshift of Au SPR energy (from 520 nm to ~650 nm) is obtained when the Au-core/CIGS-shell heterostructures are formed (Fig. 6(d)).

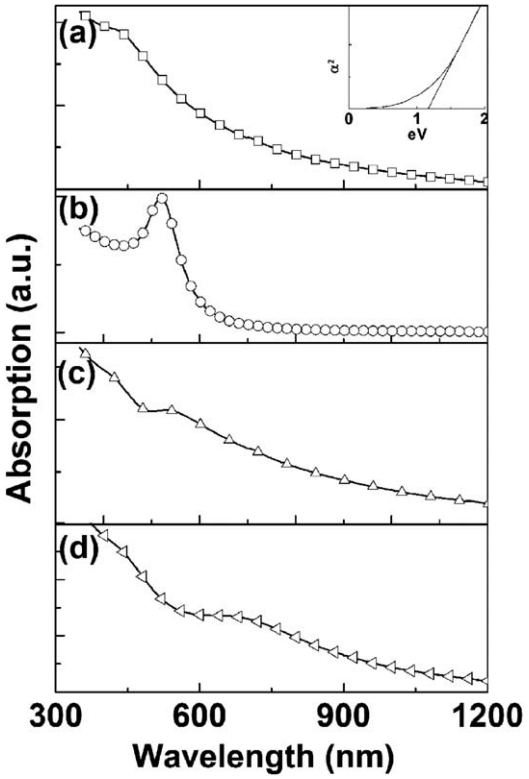

Fig. 6 Typical room-temperature UV-Visible absorbance spectra of (a) pure CIGS and band gap extrapolation (the band gap of the nanocrystals is estimated by plotting the α^2 *versus* energy and extrapolating the plot to zero α^2 as shown in the inset), (b) pure gold nps, (c) Au–CIGS side-by-side heterostructures and (d) Au-core/CIGS-shell heterostructures.

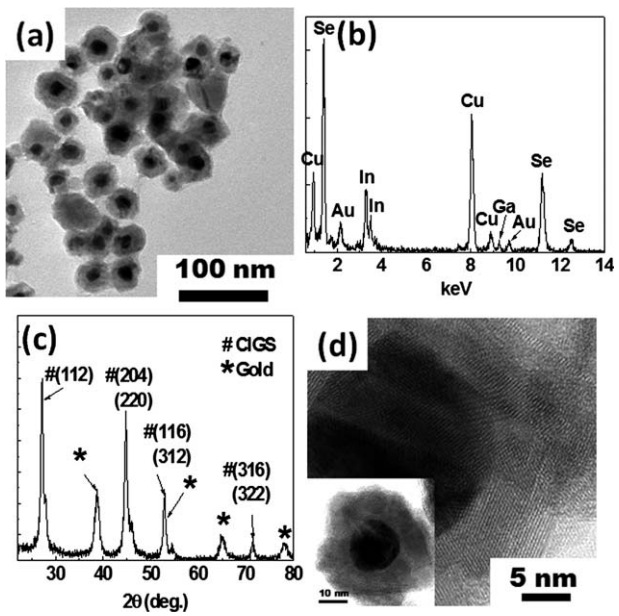

Fig. 5 (a) Low magnification TEM image of Au-core/CIGS-shell nanoparticles; (b) EDX taken from a single Au-core/CIGS-shell np (Cu TEM grid is used for the observation of Au). The composition of CIGS can be estimated from sample dispersed on a Au TEM grid (Fig. S1(b)†); (c) XRD taken from the powder of Au-core/CIGS-shell nps; and (d) magnified TEM image of one Au-core/CIGS-shell np.

Discussions

The observation of (112) planes serving as the predominant termination surface for most of the CIGS nanoparticles is not surprising. It has been theoretically predicted that the (112) planes are associated with the lowest surface energy (compared to other crystalline planes in CIGS) when cation vacancies and/or In-on-Cu antisites are introduced,[19] which is very common during the CIGS crystal growth.[20] In fact, the (112) preferential textured growth has been observed in the CIGS thin film growth.[21] Consequently, such a termination surface (the crystalline (112) planes) is critical in determining the formation of the Au–CIGS side-by-side heterostructure at later stage. The atomic stacking of the (112) plane is special, *i.e.*, it is composed of layers of Cu/In and layers of Se stacked in an alternative manner (Fig. S3†). The polar (112) surface[19,22] is usually terminated with either a layer of Se or a layer of Cu and In. The finding that Au prefers to nucleate on the (112) plane, which does not match the normal crystallographic growth habit, then suggest that the Se

serves as the terminated (112) planes attracting the Au nucleation due to the preferred Au–Se bond.[23] Although literature data on heterostructured CIGS–Au are not available, it has been reported in other metal selenide–Au heterostructures that Se serves as the termination layer, leading to selective Au nanoparticle growth on that specific Se terminated surface.[24,25] Although more than one (112) plane appears at the CIGS surface, it is very likely that the surface energy of these (112) planes can differ due to different defect density/configuration of such a plane. If such hypothesis holds, then Au should choose to nucleate on the specific (112) plane with the least energy penalty. Once nucleated, further growth of the Au seems to consume less energy than nucleation, and this leads to the one-to-one couple of the Au and CIGS nanoparticle. Further increase in the amount of Au source in the solution during growth fails to lead to one CIGS-to-multiple Au nanoparticle configuration, but the growth of extremely large Au nanoparticles on the CIGS (Fig. S4†). This serves as further support for the "low growth energy" argument.

Nevertheless, as both nucleation and growth would be affected by a number of parameters that can modify either the surface energies or kinetic energy barriers, one would expect that it is controllable to achieve nanoparticle configurations from one CIGS-to-one-Au to one CIGS-to-multiple-Au. For example, by increasing the synthesis temperature, we have fabricated one CIGS-to-multiple-Au nanoparticles, and in such a case, the Au nanoparticles are found to nucleate on not only one, but multiple (112) planes, as well as other termination surfaces of CIGS such as the (200) planes (Fig. S5†).

As a comparison, although the growth pattern of the Au-core/CIGS-shell nanoparticles is distinctively different from that of the side-by-side heterostructures, the underlining physical principle that determines the nucleation and growth is similar. One shall note that as we reverse the synthesis procedure, *i.e.*, using Au nanoparticle as the seeds for further CIGS growth, the termination surface of Au nanoparticles becomes important in the nucleation process of CIGS. As most of the Au nanoparticles are spherical in shape, one shall expect little difference in the nucleation starting location. Consequently, multiple nucleation sites on the Au nanoparticle surface and the growth followed eventually lead to the formation of Au-core/CIGS-shell nanoparticle configuration.

Nanometre sized gold colloids exhibit strong surface plasmon resonance and present an absorption peak at ~520 nm. The position of the gold SPR depends on the Au particle size,[26] shape,[27] as well as the surrounding medium.[3] The observation of 20 nm redshift in SPR of the Au–CIGS side-by-side structures can be ascribed to the weak interaction between Au and CIGS dielectric *via* the small interface between the two. As a comparison, the significant redshift (from 520 nm to 650 nm) observed in the Au-core/CIGS-shell sample results from the complete embedding of the Au particles in the high dielectric constant (~13.6) CIGS.[28]

Conclusions

In summary, Au/CIGS side-by-side and core/shell nanostructures have been demonstrated using a simple seed-mediated growth method. The preferential nucleation and growth of Au on the CIGS (112) planes enables the controlled synthesis of heterostructured nanoparticles with one-Au-to-one-CIGS configuration, which can be further extended to multiple-Au-to-one-CIGS heterostructures by mildly modifying the growth temperature. On the other hand, the same thermodynamic issue determines the Au-core/CIGS-shell nanoparticle configuration when the growth process is reversed by taking Au nps as the seeds. Such morphology controllable growth methodology can be generally applied to the family of I–III–VI_2 materials (Fig. S6†), which share similar growth energetic. By manipulating the configuration of the heterostructured Au/CIGS nanoparticles, the SPR energy of the Au can be modified. This understanding provides guidance for the further designing of the coupled structures for various light energy conversion related applications.

Acknowledgements

This work is supported by grants from the GRF of HKSAR under project No. 414908, 414709, 414710, NSFC (10928408) and CUHK Focused Investment Scheme C.

Notes and references

1 R. Costi, A. E. Saunders, E. Elmalem, A. Salant and U. Banin, *Nano Lett.*, 2008, **8**, 637–641.
2 T. Hirakawa and P. V. Kamat, *Langmuir*, 2004, **20**, 5645–5647.
3 J. S. Lee, E. V. Shevchenko and D. V. Talapin, *J. Am. Chem. Soc.*, 2008, **130**, 9673–9675.
4 Y. Fu, J. Zhang and J. R. Lakowicz, *J. Am. Chem. Soc.*, 2010, **132**, 5540–5541.
5 R. Costi, A. E. Saunders and U. Banin, *Angew. Chem., Int. Ed.*, 2010, **49**, 4878–4897.
6 K. Ramanathan, M. A. Contreras, C. L. Perkins, S. Asher, F. S. Hasoon, J. Keane, D. Young, M. Romero, W. Metzger, R. Noufi, J. Ward and A. Duda, *Prog. Photovoltaics*, 2003, **11**, 225–230.
7 http://www.nrel.gov/pv/hotline/pdfs/2010_08_23-31.pdf, 2010.
8 http://www.nanosolar.com/company/blog/nanosolar-confirms-factory-expansion-and-financial-strength, 2010.
9 T. Hirakawa and P. V. Kamat, *J. Am. Chem. Soc.*, 2005, **127**, 3928–3934.
10 W. T. Chen, T. T. Yang and Y. J. Hsu, *Chem. Mater.*, 2008, **20**, 7204–7206.
11 Y. Liu, D. Li, R. Y. Zhu, G. J. You, S. X. Qian, Y. Yang and J. L. Shi, *Appl. Phys. B: Lasers Opt.*, 2003, **76**, 435–439.
12 T. T. Yang, W. T. Chen, Y. J. Hsu, K. H. Wei, T. Y. Lin and T. W. Lin, *J. Phys. Chem. C*, 2010, **114**, 11414–11420.
13 H. Yu, M. Chen, P. M. Rice, S. X. Wang, R. L. White and S. H. Sun, *Nano Lett.*, 2005, **5**, 379–382.
14 J. Tang, S. Hinds, S. O. Kelley and E. H. Sargent, *Chem. Mater.*, 2008, **20**, 6906–6910.
15 M. G. Panthani, V. Akhavan, B. Goodfellow, J. P. Schmidtke, L. Dunn, A. Dodabalapur, P. F. Barbara and B. A. Korgel, *J. Am. Chem. Soc.*, 2008, **130**, 16770–16777.
16 Z. Zhang, F. Zhou and E. J. Lavernia, *Metall. Mater. Trans. A*, 2003, **34**, 1349–1355.
17 Q. Guo, S. J. Kim, M. Kar, W. N. Shafarman, R. W. Birkmire, E. A. Stach, R. Agrawal and H. W. Hillhouse, *Nano Lett.*, 2008, **8**, 2982–2987.
18 S. H. Wei, S. B. Zhang and A. Zunger, *Appl. Phys. Lett.*, 1998, **72**, 3199–3201.
19 S. B. Zhang and S. H. Wei, *Phys. Rev. B: Condens. Matter Mater. Phys.*, 2002, **65**, 081402.
20 O. Igarashi, *Jpn. J. Appl. Phys., Part 2*, 1995, **34**, 1520–1523.
21 D. X. Liao and A. Rockett, *J. Appl. Phys.*, 2008, **104**, 094908.
22 Y. Yan, R. Noufi and M. M. Al-Jassim, *Phys. Rev. Lett.*, 2006, **96**, 205501.
23 M. S. Hussain, *J. Crystallogr. Spectrosc. Res.*, 1986, **16**, 91–99.

24 A. Salant, E. Amitay-Sadovsky and U. Banin, *J. Am. Chem. Soc.*, 2006, **128**, 10006–10007.
25 T. Mokari, E. Rothenberg, I. Popov, R. Costi and U. Banin, *Science*, 2004, **304**, 1787–1790.
26 S. Link and M. A. El-Sayed, *J. Phys. Chem. B*, 1999, **103**, 4212–4217.
27 C. L. Nehl and J. H. Hafner, *J. Mater. Chem.*, 2008, **18**, 2415–2419.
28 M. Gloeckler, A. L. Fahrenbruch and J. R. Sites, *Numerical Modeling of CIGS and CdTe Solar Cells: Setting the Baseline*, Proceedings of 3rd World Conference on Photovoltaic energy Conversion, 2003, vol. 1, pp. 491–494.